Correspondence

Optimal Sensor Placement for Dilution of Precision Minimization Via Quadratically Constrained Fractional Programming

An approach to find the global optimal solution of the dilution of precision (DOP) problem is presented. The DOP optimization problem considered assumes an environment comprising multiple randomly predeployed sensors (or navigation sources) and an additional sensor is to be introduced at the location that minimizes variations of the DOP problem (e.g., weighted geometric DOP, horizontal DOP, vertical DOP, etc.). It is shown that the DOP problem can be formulated as a quadratically constrained fractional quadratic program. An algorithm for solving this program is presented and Monte Carlo simulation results are given demonstrating convergence of the proposed approach to the global optimal solution. Additionally, Monte Carlo simulation results are presented, demonstrating the efficacy of the proposed algorithm to solving the DOP minimization problem versus using nonlinear numerical optimization solvers, which often converge to local optima. Also, the superiority of the proposed approach is demonstrated against other approaches that approximate the DOP minimization problem.

I. INTRODUCTION

Optimal sensor placement is crucial in many application domains including source localization, tracking, and navigation [1]–[3]. In source localization and target tracking applications, one is interested in optimally placing the sensor, which makes observations to an unknown source (e.g., emitter) or target, minimizing the estimation error uncertainty about the state of the sensor or target [4]–[6]. In navigation applications, one is interested in optimally placing the sensor (e.g., receiver), which makes observations to known sources (e.g., global navigation satellite system (GNSS) satellites or signal of opportunity (SOP) transmitters), minimizing the estimator error uncertainty about the sensor's state [7]–[9]. Several metrics have been defined as cost functions to be optimized, most notably first, minimizing the geometric dilution of precision (GDOP) or more generally the weighted GDOP (WGDOP), which is equivalent to minimizing the trace of the estimation error covariance matrix [10]–[15] and second, maximizing the determinant of the GDOP or WGDOP matrix, which is

Manuscript received December 6, 2017; revised June 12, 2018 and August 9, 2018; released for publication August 14, 2018. Date of publication November 9, 2018; date of current version August 7, 2019.

DOI. No. 10.1109/TAES.2018.2879552

Refereeing of this contribution was handled by D. Qiu.

This work was supported in part by the National Science Foundation under Grant 1566240.

Authors' addresses: J. J. Khalife and Z. M. Kassas are with the Department of Electrical and Computer Engineering, University of California, Riverside, CA 92521 USA, (E-mail: jkhal001@ucr.edu; zkassas@ieee.org). *(Corresponding author: Zaher M. Kassas.)*

0018-9251 © 2018 IEEE

equivalent to maximizing the determinant of the Fisher information matrix [2], [16]. However, all the aforementioned optimization problems are nonconvex, necessitating the use of numerical general-purpose optimization solvers, which tend to be computationally intensive and could converge to a local optimum.

Instead of directly optimizing a functional of the WGDOP matrix, alternative approximating metrics were proposed, such as maximizing the area of the polygon whose vertices are the endpoints of the unit line-of-sight (LOS) vectors from the source to the sensor [17]. In [18], it was shown that this criterion was piecewise concave for the problem of placing an additional sensor to a set of predeployed sensors localizing a *single* source using pseudorange measurements, and a closed-form expression for the optimal two-dimensional (2-D) position of the additional sensor was derived. The problem was generalized to the case of localizing *multiple* sources and it was shown that optimizing the product of areas yielded a set of parallelizable convex programs [19].

This paper considers the following two equivalent problems. The first problem assumes an environment comprising multiple randomly predeployed sensors that are collaboratively localizing an unknown source using range or pseudorange measurements. In certain practical scenarios, the sensors could be prevented from moving to more favorable locations to reduce the uncertainty about the source's estimated position, and it could be more efficient to deploy an additional collaborating sensor. The second problem assumes a receiver navigating with pseudorange measurements from multiple GNSS satellites and terrestrial SOPs. This paper addresses the questions of what is the optimal location to place the additional sensor and what is the optimal location that the receiver should place itself? Here, optimality is defined in the sense of minimizing the WGDOP or elements within the WGDOP matrix, e.g., weighted horizontal dilution of precision (WHDOP), weighted vertical dilution of precision (WVDOP), and weighted time dilution of precision. In contrast to other approaches that aim to optimize other metrics that approximate GDOP [13], [20], this paper considers optimizing the WGDOP directly. To the authors' knowledge, there exists no method for obtaining the global optimal solution to this problem yet.

In order to obtain a global optimal solution, this paper shows that the WGDOP minimization problem can be formulated as a quadratically constrained fractional quadratic program, to which numerical solutions yielding the global optimum have been developed in the nonconvex optimization literature [21]. Monte Carlo (MC) simulations are presented showing that the solution obtained using the proposed method always coincides with the true global optimal solution. Simulations results are also presented demonstrating the efficacy of the proposed approach to solving the WGDOP minimization problem versus using general-purpose nonlinear numerical optimization solvers, which often converge to local optima. Also, the superiority of the proposed approach is demonstrated against other approaches that approximate the DOP minimization problem.

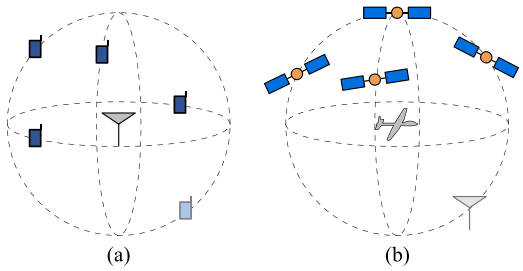

Fig. 1. Two motivating examples. (a) Placing an additional sensor for optimal source localization. (b) Solving for relative SOP position to minimize VDOP or WVDOP.

The remainder of this paper is organized as follows. Section II presents two motivating problems considered by this paper. Section III formulates the sensor placement problem and describes the models employed in this paper. Section IV proposes a method for solving the DOP minimization problem. Section V presents simulation results validating the proposed approach. Concluding remarks are given in Section VI.

II. MOTIVATING PROBLEMS

This paper addresses two equivalent problems. The first problem, illustrated in Fig. 1(a), considers a number of sensors (e.g., receivers) that are predeployed in some random configuration, which are collaboratively localizing a stationary source (e.g., emitter) by making pseudorange observations to this source. A central estimator is used to fuse pseudoranges from all sensors to estimate the source's 3-D position and its clock bias. Where should an additional sensor be placed so to minimize the WGDOP? If this additional sensor is a moving agent, where should it move to next?

The second problem, illustrated in Fig. 1(b), considers an unmanned aerial vehicle (UAV) that is navigating via GNSS signals, but whose navigation solution suffers from a large vertical dilution of precision (VDOP) or WVDOP. This problem is inherent to GNSS-based navigation, due to the geometric configuration of GNSS satellites being above the UAV. It has been demonstrated that utilizing terrestrial SOP transmitters significantly reduces the VDOP or WVDOP, since now the elevation angle from which the signals are received spans -90° to $+90^\circ$ [20], [22], [23]. In such environment, where should the UAV position itself in order to minimize its VDOP or WVDOP?

At the core, these problems are identical: they both boil down to minimizing the WGDOP or elements within the WGDOP matrix over a unit vector that corresponds to the relative position vector between the additional sensor (navigation source) and the source (UAV). In order to solve these problems, this paper first formulates the core WGDOP minimization problem as a quadratically constrained fractional quadratic program, to which numerical solutions yielding the global optimum have been developed in the

nonconvex optimization literature [21]. Next, the algorithm for solving this minimization problem is detailed. Then, MC simulations for the two DOP minimization problems illustrated in Fig. 1 along with numerical convergence and complexity analyses associated with the proposed approach versus existing approaches are provided. An additional application of the proposed approach for source localization with a mobile agent is also presented.

III. MODEL DESCRIPTION AND PROBLEM FORMULATION

In this section, the models adopted in this paper are described and the DOP minimization problem is subsequently formulated.

A. Model Description

The state to be estimated is $\boldsymbol{\eta} \triangleq [\boldsymbol{r}_s^{\mathrm{T}}, c\delta t_s]^{\mathrm{T}}$, which is composed of the 3-D position vector $\boldsymbol{r}_s \triangleq [x_s, y_s, z_s]^{\mathrm{T}}$ of the source (UAV) and its clock bias $c\delta t_s$ expressed in meters, where c is the speed of light and δt_s is the source's (UAV's) clock bias expressed in seconds. A prior for $\boldsymbol{\eta}$ may be given, denoted by $\hat{\boldsymbol{\eta}}$, with the associated initial covariance $\mathbf{P}_0 \succ \mathbf{0}$. The position vector of the jth sensor (navigation source) is given by $\boldsymbol{r}_{r_j} \triangleq [x_{r_j}, y_{r_j}, z_{r_j}]^{\mathrm{T}}$ and its clock bias by $c\delta t_{r_j}$, $j = 1, \ldots, N$, where $N \geq 5$ is the total number of sensors (navigation sources). It is assumed that the positions and clock biases of all the sensors (navigation sources) are known at any time-step. Moreover, each sensor is making a pseudorange measurement to the source. Alternatively, the UAV is making pseudorange measurements to each navigation source. The pseudorange measurements may be expressed as follows:

$$z_j = \left\| \boldsymbol{r}_{r_j} - \boldsymbol{r}_s \right\|_2 + c \cdot \left[\delta t_{r_j} - \delta t_s \right] + v_j$$

where $\boldsymbol{v} \triangleq [v_1, \ldots, v_N]^{\mathrm{T}}$ is the measurement noise vector, which is modeled as a zero-mean Gaussian random vector with covariance $\mathbf{R}_N$ [24]. Note that the measurement noise may be correlated; hence, $\mathbf{R}_N$ is an arbitrary symmetric positive-definite matrix. In the case of the navigation sources being GNSS satellites, it is assumed that z_j has been corrected for ionospheric and tropospheric delays. The Jacobian matrix $\mathbf{H}_N$ of the measurement vector $\boldsymbol{z} \triangleq [z_1, \ldots, z_N]^{\mathrm{T}}$ is given by

$$\mathbf{H}_N = [\boldsymbol{h}_1 \quad \ldots \quad \boldsymbol{h}_N]^{\mathrm{T}}, \quad \boldsymbol{h}_j \triangleq \left[\frac{\boldsymbol{r}_s^{\mathrm{T}} - \boldsymbol{r}_{r_j}^{\mathrm{T}}}{\left\| \boldsymbol{r}_s - \boldsymbol{r}_{r_j} \right\|_2}, -1 \right]^{\mathrm{T}}.$$

Subsequently, the estimation error covariance matrix of a weighted nonlinear least-squares (WNLS) estimator with N sensors (navigation sources), denoted $\mathbf{P}_N$, is given by

$$\mathbf{P}_N \triangleq \left(\mathbf{P}_0^{-1} + \mathbf{H}_N^{\mathrm{T}} \mathbf{R}_N^{-1} \mathbf{H}_N \right)^{-1}.$$

B. Problem Formulation

The problem addressed in this paper is the optimal placement of an additional sensor (navigation source) to a set of $N - 1 \geq 4$ predeployed sensors (navigation sources)

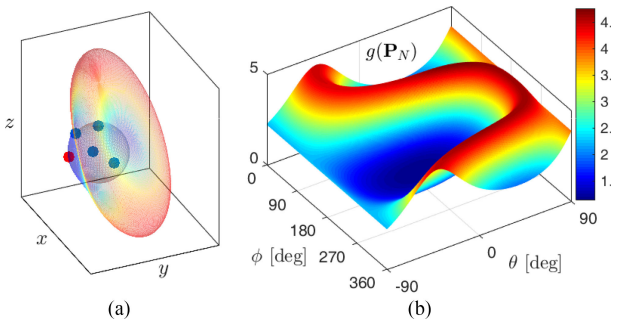

Fig. 2. Visualization of $g(\mathbf{P}_N) = \mathrm{tr}[\mathbf{P}_N]$. (a) 3-D pattern plot where $g(\mathbf{P}_N)$ is proportional to the radial distance to the 3-D surface and the corresponding sensor location is its projection onto the unit sphere. The dark blue markers indicate the endpoints of the unit LOS vectors to four predeployed sensors. The red marker indicates the endpoint of the vector $\boldsymbol{x}$ that minimizes $g(\mathbf{P}_N)$. (b) Surface plot showing $g(\mathbf{P}_N)$ as a function of the azimuth angle ϕ and elevation angle θ.

in order to optimize a functional of the localization (navigation solution) estimation error covariance. To this end, two cost functions are defined

$$g\left(\mathbf{P}_N\right) \triangleq \mathrm{tr}\left[\mathbf{T}\mathbf{P}_N\mathbf{T}^{\mathrm{T}}\right], \qquad g'\left(\mathbf{P}_N\right) \triangleq \det\left[\mathbf{T}'\mathbf{P}_N\mathbf{T}'^{\mathrm{T}}\right],$$

where $\mathrm{tr}[\cdot]$ is the matrix trace, $\det[\cdot]$ is the matrix determinant, $\mathbf{T}$ is an arbitrary $L \times 4$ matrix and L is a positive integer, and $\mathbf{T}'$ is an arbitrary $L' \times 4$ matrix with rank L' and L' is a positive integer with $0 < L' \leq 4$. These conditions on $\mathbf{T}'$ ensure that $g'(\mathbf{P}_N)$ is nonzero. Note that $\mathbf{H}_N = [\mathbf{H}_{N-1}^{\mathrm{T}} \quad \boldsymbol{h}_N]^{\mathrm{T}}$ and $\{\boldsymbol{r}_{r_j}\}_{j=1}^{N-1}$ and $\boldsymbol{r}_s$ are fixed. Therefore, $\mathbf{H}_{N-1}$ is constant. The problem is to find $\boldsymbol{r}_{r_N}$ that minimizes $g(\mathbf{P}_N)$ or $g'(\mathbf{P}_N)$. The vector $\boldsymbol{h}_N$ may be expressed as $\boldsymbol{h}_N = [\boldsymbol{x}^{\mathrm{T}} \quad -1]^{\mathrm{T}}$ where $\boldsymbol{x} \triangleq \frac{\boldsymbol{r}_s - \boldsymbol{r}_{r_N}}{\|\boldsymbol{r}_s - \boldsymbol{r}_{r_N}\|_2}$ is the unit LOS vector from the source (UAV) to the Nth sensor (navigation source). One can parameterize $\boldsymbol{x}$ in terms of the elevation angle θ and the azimuth angle ϕ according to

$$\boldsymbol{x} = [\cos\theta\,\cos\phi \quad \cos\theta\,\sin\phi \quad \sin\theta]^{\mathrm{T}}$$

where $-\frac{\pi}{2} \leq \theta \leq \frac{\pi}{2}$ and $0 \leq \phi < 2\pi$. It can be seen that any sensor (navigation source) position on the ray whose direction is given by $\boldsymbol{x}$ yields the same estimation error covariance. Subsequently, the problem boils down to finding the vector $\boldsymbol{x}$ on the unit sphere that minimizes $g(\mathbf{P}_N)$ or $g'(\mathbf{P}_N)$, given by the following optimization problems:

$$\underset{\boldsymbol{x}^{\mathrm{T}}\boldsymbol{x}=1}{\text{minimize}} \quad g(\mathbf{P}_N) = \mathrm{tr}\left[\mathbf{T}\mathbf{P}_N\mathbf{T}^{\mathrm{T}}\right] \tag{1}$$

$$\underset{\boldsymbol{x}^{\mathrm{T}}\boldsymbol{x}=1}{\text{minimize}} \quad g'(\mathbf{P}_N) = \det\left[\mathbf{T}'\mathbf{P}_N\mathbf{T}'^{\mathrm{T}}\right]. \tag{2}$$

In the rest of this paper, these two problems are generally referred to as the DOP minimization problem. In order to visualize $g(\mathbf{P}_N)$ and $g'(\mathbf{P}_N)$, the following two motivating examples are considered.

In the first example, four sensors are randomly placed on the unit sphere, which was gridded by uniformly sampling the domain of $\theta \in [-\frac{\pi}{2}, \frac{\pi}{2}]$ and $\phi \in [0, 2\pi)$. Next, $g(\mathbf{P}_N)$ and $g'(\mathbf{P}_N)$ were evaluated for $\mathbf{T} = \mathbf{T}' = \mathbf{I}$ at each (θ, ϕ) pair and were plotted in two ways as shown in Figs. 2 and 3: (a) as a 3-D pattern plot where $g(\mathbf{P}_N)$ and $g'(\mathbf{P}_N)$ are

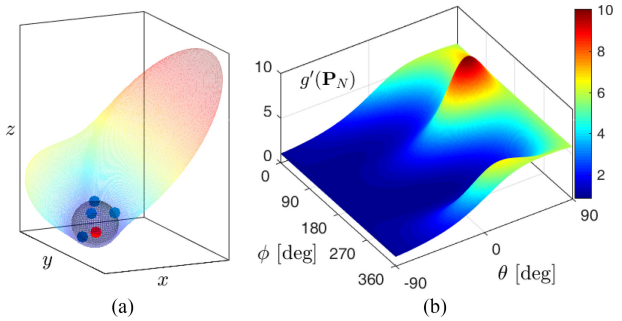

Fig. 3. Visualization of $g'(\mathbf{P}_N) = \det[\mathbf{P}_N]$. (a) 3-D pattern plot where $g'(\mathbf{P}_N)$ is proportional to the radial distance to the 3-D surface and the corresponding sensor location is its projection onto the unit sphere. The dark blue markers indicate the endpoints of the unit LOS vectors to four predeployed sensors. The red marker indicates the endpoint of the vector $\boldsymbol{x}$ that minimizes $g'(\mathbf{P}_N)$. (b) Surface plot showing $g'(\mathbf{P}_N)$ as a function of the azimuth angle ϕ and elevation angle θ.

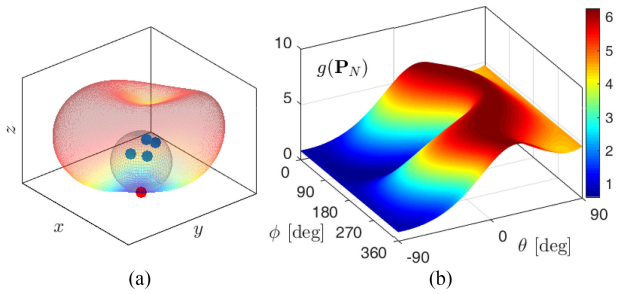

Fig. 4. Visualization of $g(\mathbf{P}_N) = \boldsymbol{e}_3^{\mathrm{T}}\mathbf{P}_N\boldsymbol{e}_3$. (a) 3-D pattern plot where the VDOP $g(\mathbf{P}_N)$ is proportional to the radial distance to the 3-D surface and the corresponding sensor location is its projection onto the unit sphere. The dark blue markers indicate the endpoints of the unit LOS vectors to four GNSS satellites. The red marker indicates the endpoint of the vector $\boldsymbol{x}$ that minimizes the WVDOP. (b) Surface plot showing the WVDOP as a function of the azimuth angle ϕ and elevation angle θ.

proportional to the radial distance to the 3-D surface and the corresponding sensor location is its projection onto the unit sphere and (b) as a surface plot as a function of the azimuth and elevation angles. It can be seen from Figs. 2 and 3 that $g(\mathbf{P}_N)$ and $g'(\mathbf{P}_N)$ are nonconvex and have several maxima and minima.

In the second example, a UAV is assumed to have access to four GNSS satellites. The satellite elevation mask was set to 10°, i.e., satellites below such elevation mask are not used to produce the navigation solution (this is common in GNSS-based navigation to avoid severely attenuated GNSS signals and multipath). The UAV is trying for solve its relative position to a terrestrial SOP in order to minimize its VDOP, given by $g(\mathbf{P}_N) = \mathrm{tr}[\boldsymbol{e}_3^{\mathrm{T}}\mathbf{P}_N\boldsymbol{e}_3] = \boldsymbol{e}_3^{\mathrm{T}}\mathbf{P}_N\boldsymbol{e}_3$, where $\boldsymbol{e}_3 \triangleq [0, 0, 1, 0]^{\mathrm{T}}$. Note that the distance to the GNSS satellites is significantly large such that the unit LOS vectors form the UAV to the satellites do not change while the UAV is positioning itself with respect to the SOP. Hence, this problem becomes equivalent to the sensor placement problem whose solution is the desired relative position of the SOP with respect to the UAV. This scenario is illustrated in Fig. 4, where the dark blue marks indicate the endpoints of the unit LOS vectors to the four GNSS satellites and the red mark indicates the relative position of the SOP that minimizes the WVDOP. Since $\boldsymbol{e}_3^{\mathrm{T}}\mathbf{P}_N\boldsymbol{e}_3$ is a scalar, then $g(\mathbf{P}_N) = g'(\mathbf{P}_N)$. Subsequently, only $g(\mathbf{P}_N)$ is plotted. It can be seen from Fig. 4 that $g(\mathbf{P}_N)$ (and consequently $g'(\mathbf{P}_N)$) is nonconvex and has several local minima and maxima.

In the next section, a method for obtaining the global minimum of $g(\mathbf{P}_N)$ is developed.

IV. DOP MINIMIZATION

In this section, the minimization problems (1) and (2) are formulated as quadratically constrained fractional quadratic programs and the global solutions are subsequently discussed.

A. DOP Minimization as a Quadratically Constrained Fractional Quadratic Program

Let the measurement noise covariance $\mathbf{R}_N$ after placing the Nth sensor (navigation source) have the following partitioning:

$$\mathbf{R}_N = \begin{bmatrix} \mathbf{R}_{N-1} & \boldsymbol{r}_N \\ \boldsymbol{r}_N^{\mathrm{T}} & \sigma_N^2 \end{bmatrix}.$$

Let its inverse $\mathbf{Y}_N$ be partitioned according to

$$\mathbf{Y}_N \triangleq \mathbf{R}_N^{-1} = \begin{bmatrix} \mathbf{Y}_{N-1} & \boldsymbol{y}_N \\ \boldsymbol{y}_N^{\mathrm{T}} & \mu_N^2 \end{bmatrix}.$$

The estimation error covariance matrix after placing the Nth sensor (navigation source) may then be expressed as

$$\begin{aligned} \mathbf{P}_N &\triangleq \left(\mathbf{P}_0^{-1} + \mathbf{H}_N^{\mathrm{T}}\mathbf{R}_N^{-1}\mathbf{H}_N\right)^{-1} \\ &= \left(\mathbf{P}_0^{-1} + \mathbf{H}_{N-1}^{\mathrm{T}}\mathbf{Y}_{N-1}\mathbf{H}_{N-1} + \mu_N^2\boldsymbol{h}_N\boldsymbol{h}_N^{\mathrm{T}}\right. \\ &\quad \left. + \boldsymbol{h}_N\boldsymbol{y}_N^{\mathrm{T}}\mathbf{H}_{N-1} + \mathbf{H}_{N-1}^{\mathrm{T}}\boldsymbol{y}_N\boldsymbol{h}_N^{\mathrm{T}}\right)^{-1} \\ &= \left(\mathbf{M} + \boldsymbol{u}\boldsymbol{u}^{\mathrm{T}}\right)^{-1} \end{aligned} \tag{3}$$

where $\boldsymbol{u} \triangleq \mu_N\boldsymbol{h}_N + \frac{1}{\mu_N}\mathbf{H}_{N-1}^{\mathrm{T}}\boldsymbol{y}_N$ and $\mathbf{M} \triangleq \mathbf{P}_0^{-1} + \mathbf{H}_{N-1}^{\mathrm{T}}(\mathbf{Y}_{N-1} - \frac{1}{\mu_N^2}\boldsymbol{y}_N\boldsymbol{y}_N^{\mathrm{T}})\mathbf{H}_{N-1}$. Using the matrix inversion lemma, it can be shown that $\mathbf{M} = \mathbf{P}_0^{-1} + \mathbf{H}_{N-1}^{\mathrm{T}}\mathbf{R}_{N-1}^{-1}\mathbf{H}_{N-1}$. If a prior is available, then $\mathbf{H}_{N-1}$ does not need to be full column rank. If no prior is available, then $\mathbf{M} = \mathbf{H}_{N-1}^{\mathrm{T}}\mathbf{R}_{N-1}^{-1}\mathbf{H}_{N-1}$, in which case $\mathbf{H}_{N-1}$ must be full column rank. Either way, $\mathbf{M}$ is positive definite and so is its inverse. Using the matrix inversion lemma, $\mathbf{P}_N$ may be expressed as

$$\mathbf{P}_N = \mathbf{M}^{-1} - \frac{\mathbf{M}^{-1}\boldsymbol{u}\boldsymbol{u}^{\mathrm{T}}\mathbf{M}^{-1}}{1 + \boldsymbol{u}^{\mathrm{T}}\mathbf{M}^{-1}\boldsymbol{u}}. \tag{4}$$

Next, $g(\mathbf{P}_N)$ and $g'(\mathbf{P}_N)$ are re-expressed as fractional quadratic cost functions.

1) *Trace Minimization:* Using (4), $g(\mathbf{P}_N)$ may be expressed as

$$g\left(\mathbf{P}_N\right) = C - \frac{\mathrm{tr}\left[\mathbf{T}\mathbf{M}^{-1}\boldsymbol{u}\boldsymbol{u}^{\mathrm{T}}\mathbf{M}^{-1}\mathbf{T}^{\mathrm{T}}\right]}{1 + \boldsymbol{u}^{\mathrm{T}}\mathbf{M}^{-1}\boldsymbol{u}}$$

where $C \triangleq \text{tr}[\mathbf{T}\mathbf{M}^{-1}\mathbf{T}^{\mathsf{T}}]$. Using the cyclic properties of the trace, the cost function may be expressed as

$$g(\mathbf{P}_N) = C + \frac{\boldsymbol{u}^{\mathsf{T}}\mathbf{Q}\boldsymbol{u}}{1+\boldsymbol{u}^{\mathsf{T}}\mathbf{M}^{-1}\boldsymbol{u}} \tag{5}$$

where $\mathbf{Q} \triangleq -\mathbf{M}^{-1}\mathbf{T}^{\mathsf{T}}\mathbf{T}\mathbf{M}^{-1}$. Note that $\boldsymbol{h}_N = [\boldsymbol{x}^{\mathsf{T}}, -1]^{\mathsf{T}}$ and let $\mathbf{Q}$, $\mathbf{M}^{-1}$, $\boldsymbol{\zeta} \triangleq \mathbf{Q}\mathbf{H}_{N-1}^{\mathsf{T}}\boldsymbol{y}_N$, and $\boldsymbol{\psi} \triangleq \mathbf{M}^{-1}\mathbf{H}_{N-1}^{\mathsf{T}}\boldsymbol{y}_N$ have the following partitioning:

$$\mathbf{Q} = \begin{bmatrix} \bar{\mathbf{A}}_1 & \bar{\boldsymbol{b}}_1 \\ \bar{\boldsymbol{b}}_1^{\mathsf{T}} & \bar{c}_1 \end{bmatrix}, \mathbf{M}^{-1} = \begin{bmatrix} \bar{\mathbf{A}}_2 & \bar{\boldsymbol{b}}_2 \\ \bar{\boldsymbol{b}}_2^{\mathsf{T}} & \bar{c}_2 \end{bmatrix}, \boldsymbol{\zeta} = \begin{bmatrix} \boldsymbol{\zeta}_1 \\ \zeta_2 \end{bmatrix}, \boldsymbol{\psi} = \begin{bmatrix} \boldsymbol{\psi}_1 \\ \psi_2 \end{bmatrix}.$$

Then, $g(\mathbf{P}_N)$ may be expressed as

$$g(\mathbf{P}_N) = g(\boldsymbol{x}) \triangleq C + \frac{g_1(\boldsymbol{x})}{g_2(\boldsymbol{x})}$$

where $g_n(\boldsymbol{x}) \triangleq \boldsymbol{x}^{\mathsf{T}}\mathbf{A}_n\boldsymbol{x} - 2\boldsymbol{b}_n^{\mathsf{T}}\boldsymbol{x} + c_n$, $n = 1, 2$, and

$$\begin{aligned}
\mathbf{A}_1 &\triangleq \mu_N^2\bar{\mathbf{A}}_1 \\
\boldsymbol{b}_1 &\triangleq \mu_N^2\bar{\boldsymbol{b}}_1 - \boldsymbol{\zeta}_1 \\
c_1 &\triangleq \mu_N^2\bar{c}_1 + \frac{1}{\mu_N^2}\boldsymbol{y}_N^{\mathsf{T}}\mathbf{H}_{N-1}\mathbf{Q}\mathbf{H}_{N-1}^{\mathsf{T}}\boldsymbol{y}_N - 2\zeta_2 \\
\mathbf{A}_2 &\triangleq \mu_N^2\bar{\mathbf{A}}_2 \\
\boldsymbol{b}_2 &\triangleq \mu_N^2\bar{\boldsymbol{b}}_2 - \boldsymbol{\psi}_1 \\
c_2 &\triangleq \mu_N^2\bar{c}_2 + \frac{1}{\mu_N^2}\boldsymbol{y}_N^{\mathsf{T}}\mathbf{H}_{N-1}\mathbf{M}^{-1}\mathbf{H}_{N-1}^{\mathsf{T}}\boldsymbol{y}_N - 2\psi_2 + 1.
\end{aligned}$$

Subsequently, the DOP minimization problem in (1) may be posed as

$$\underset{\boldsymbol{x}\in\mathcal{F}}{\text{minimize}} \quad g(\boldsymbol{x}) \tag{6}$$

where $\mathcal{F} = \{\boldsymbol{x} \in \mathbb{R}^3 : \boldsymbol{x}^{\mathsf{T}}\boldsymbol{x} = 1\}$.

2) *Determinant Minimization:* Using (4) and Sylvester's determinant theorem, $g'(\mathbf{P}_N)$ may be expressed as

$$g'(\mathbf{P}_N) = C'\left(1 + \frac{\boldsymbol{u}^{\mathsf{T}}\mathbf{Q}'\boldsymbol{u}}{1+\boldsymbol{u}^{\mathsf{T}}\mathbf{M}^{-1}\boldsymbol{u}}\right) \tag{7}$$

where $\mathbf{Q}' \triangleq -\mathbf{M}^{-1}\mathbf{T}'^{\mathsf{T}}(\mathbf{T}'\mathbf{M}^{-1}\mathbf{T}'^{\mathsf{T}})^{-1}\mathbf{T}'\mathbf{M}^{-1}$ and $C' \triangleq \det[\mathbf{T}'\mathbf{M}^{-1}\mathbf{T}'^{\mathsf{T}}]$. Let $\mathbf{Q}'$ and $\boldsymbol{\zeta}' \triangleq \mathbf{Q}'\mathbf{H}_{N-1}^{\mathsf{T}}\boldsymbol{y}_N$ have the following partitioning:

$$\mathbf{Q}' = \begin{bmatrix} \bar{\mathbf{A}}_1' & \bar{\boldsymbol{b}}_1' \\ \bar{\boldsymbol{b}}_1'^{\mathsf{T}} & \bar{c}_1' \end{bmatrix}, \quad \boldsymbol{\zeta}' = \begin{bmatrix} \boldsymbol{\zeta}_1' \\ \zeta_2' \end{bmatrix}.$$

Then, $g'(\mathbf{P}_N)$ may be expressed as

$$g'(\mathbf{P}_N) = g'(\boldsymbol{x}) \triangleq C' + \frac{g_1'(\boldsymbol{x})}{g_2(\boldsymbol{x})}$$

where $g_1'(\boldsymbol{x}) \triangleq \boldsymbol{x}^{\mathsf{T}}\mathbf{A}_1'\boldsymbol{x} - 2\boldsymbol{b}'^{\mathsf{T}}_1\boldsymbol{x} + c_1'$, and

$$\begin{aligned}
\mathbf{A}_1' &\triangleq \mu_N^2\bar{\mathbf{A}}_1' \\
\boldsymbol{b}_1' &\triangleq \mu_N^2\bar{\boldsymbol{b}}_1' - \boldsymbol{\zeta}_1' \\
c_1' &\triangleq \mu_N^2\bar{c}_1' + \frac{1}{\mu_N^2}\boldsymbol{y}_N^{\mathsf{T}}\mathbf{H}_{N-1}\mathbf{Q}'\mathbf{H}_{N-1}^{\mathsf{T}}\boldsymbol{y}_N - 2\zeta_2'.
\end{aligned}$$

Subsequently, the DOP minimization problem in (2) may be posed as

$$\underset{\boldsymbol{x}\in\mathcal{F}}{\text{minimize}} \quad g'(\boldsymbol{x}). \tag{8}$$

Note that (6) and (8) are of the form

$$\underset{\boldsymbol{x}\in\mathcal{F}}{\text{minimize}} \quad f(\boldsymbol{x}) = C_0 + \frac{f_1(\boldsymbol{x})}{f_2(\boldsymbol{x})} \tag{9}$$

where $f(\boldsymbol{x})$, $f_1(\boldsymbol{x})$, $f_2(\boldsymbol{x})$, and C_0 can be either $g(\boldsymbol{x})$, $g_1(\boldsymbol{x})$, $g_2(\boldsymbol{x})$, and C; or $g'(\boldsymbol{x})$, $g_1'(\boldsymbol{x})$, $g_2(\boldsymbol{x})$, and C', respectively.

REMARK: Note that this analysis is readily extendable to range measurements instead of pseudorange, i.e., $z_j = \|\boldsymbol{r}_{r_j} - \boldsymbol{r}_s\| + v_j$. In this case, $\mathbf{A}_n$, $\boldsymbol{b}_n$, c_n, $\mathbf{A}_n'$, $\boldsymbol{b}_n'$, and c_n' for $n = 1, 2$ become

$$\begin{aligned}
\mathbf{A}_1 &\triangleq \mu_N^2\mathbf{Q} \\
\boldsymbol{b}_1 &\triangleq -\mathbf{Q}\mathbf{H}_{N-1}^{\mathsf{T}}\boldsymbol{y}_N \\
c_1 &\triangleq \frac{1}{\mu_N^2}\boldsymbol{y}_N^{\mathsf{T}}\mathbf{H}_{N-1}\mathbf{Q}\mathbf{H}_{N-1}^{\mathsf{T}}\boldsymbol{y}_N \\
\mathbf{A}_2 &\triangleq \mu_N^2\mathbf{M}^{-1} \\
\boldsymbol{b}_2 &\triangleq -\mathbf{M}^{-1}\mathbf{H}_{N-1}^{\mathsf{T}}\boldsymbol{y}_N \\
c_2 &\triangleq \frac{1}{\mu_N^2}\boldsymbol{y}_N^{\mathsf{T}}\mathbf{H}_{N-1}\mathbf{M}^{-1}\mathbf{H}_{N-1}^{\mathsf{T}}\boldsymbol{y}_N + 1. \\
\mathbf{A}_1' &\triangleq \mu_N^2\mathbf{Q}' \\
\boldsymbol{b}_1' &\triangleq -\mathbf{Q}'\mathbf{H}_{N-1}^{\mathsf{T}}\boldsymbol{y}_N \\
c_1' &\triangleq \frac{1}{\mu_N^2}\boldsymbol{y}_N^{\mathsf{T}}\mathbf{H}_{N-1}\mathbf{Q}'\mathbf{H}_{N-1}^{\mathsf{T}}\boldsymbol{y}_N.
\end{aligned}$$

B. Domain Approximation

Although (9) minimizes the ratio of two quadratic forms, it is not a quadratically constrained fractional quadratic program due to the feasible domain. As discussed in [21], the constraint was shown to take the form

$$C_1^2 \le \boldsymbol{x}^{\mathsf{T}}\mathbf{G}\boldsymbol{x} \le C_2^2 \tag{10}$$

where $C_2^2 > C_1^2 \ge 0$ and $\mathbf{G}$ is a positive definite matrix. In what follows, a method for transforming the constraint in (9) into the form of (10) is presented.

First, it must be established that $f(\boldsymbol{x})$ is continuous. It can be seen from (5) and (7) that both denominators are greater than one since $\mathbf{M}^{-1} \succ 0$, i.e., $g_2(\boldsymbol{x}) \ge 1$ and $g_2'(\boldsymbol{x}) \ge 1$. Consequently $f(\boldsymbol{x})$ is continuous. Next, denote $\boldsymbol{x}_0^\star$ the true optimal solution of (9). Since $f(\boldsymbol{x})$ is continuous, then for every $\delta_0 > 0$ where $\|\boldsymbol{x} - \boldsymbol{x}_0^\star\|_2 < \delta_0$, there exists $\epsilon_0 > 0$ such that $|f(\boldsymbol{x}) - f(\boldsymbol{x}_0^\star)| < \epsilon_0$. Now, let $\epsilon_0 \equiv \epsilon^\star < \min_{x\in\mathcal{L}} \quad |f(\boldsymbol{x}) - f(\boldsymbol{x}_0^\star)|$, where $\mathcal{L}$ is the set of local minima on $\mathcal{F}$ excluding $\boldsymbol{x}_0^\star$. Therefore, there exists $\delta^\star$ such that $\|\boldsymbol{x} - \boldsymbol{x}_0^\star\|_2 < \delta^\star$. In order to satisfy the form of the constraint given in (10), the set $\mathcal{F}$ is approximated with

$$\mathcal{F}_2 = \left\{\boldsymbol{x} \in \mathbb{R}^3 : 1 \le \boldsymbol{x}^{\mathsf{T}}\boldsymbol{x} \le 1 + \delta\right\} \tag{11}$$

where $\delta > 0$ is made infinitely small. This approximation is needed to formulate the DOP minimization problem as the quadratically constrained fractional quadratic problem

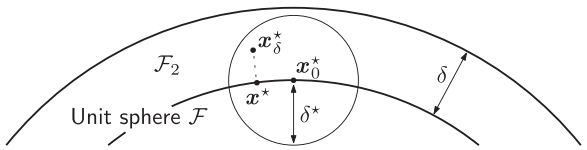

Fig. 5. Visualization of $\mathcal{F}$ and $\mathcal{F}_2$ and the relationship between $\boldsymbol{x}^\star$, $\boldsymbol{x}^\star_0$, and $\boldsymbol{x}^\star_\delta$.

discussed in the next section. It can be seen that

$$\lim_{\delta\to 0}\mathcal{F}_2=\mathcal{F}.$$

Denote $\boldsymbol{x}^\star_\delta$ the solution to

$$\underset{\boldsymbol{x}\in\mathcal{F}_2}{\text{minimize}}\quad f(\boldsymbol{x}).$$

Since $\mathcal{F}_2$ is not strictly the unit sphere, then $\boldsymbol{x}^\star_\delta$ may not be a unit vector. Define $\boldsymbol{x}^\star$ to be a unit vector along $\boldsymbol{x}^\star_\delta$ as

$$\boldsymbol{x}^\star\triangleq\frac{\boldsymbol{x}^\star_\delta}{\left\|\boldsymbol{x}^\star_\delta\right\|_2}. \tag{12}$$

This vector $\boldsymbol{x}^\star$ will be shown to converge to the optimal solution of (9) $\boldsymbol{x}^\star_0$. Let δ be small enough such that $\|\boldsymbol{x}^\star_0-\boldsymbol{x}^\star_\delta\|_2<\delta^\star$. Moreover, it can be seen from Fig. 5 that $\|\boldsymbol{x}^\star_0-\boldsymbol{x}^\star\|_2<\|\boldsymbol{x}^\star_0-\boldsymbol{x}^\star_\delta\|_2$ since $\boldsymbol{x}^\star$ is the projection of $\boldsymbol{x}^\star_\delta$ onto the unit sphere.

Consequently, for a sufficiently small δ, the following holds:

$$\left\|\boldsymbol{x}^\star_0-\boldsymbol{x}^\star\right\|_2<\delta^\star\quad\Rightarrow\quad\left|f\left(\boldsymbol{x}^\star_0\right)-f\left(\boldsymbol{x}^\star\right)\right|<\epsilon^\star$$

implying that $\boldsymbol{x}^\star$ converges to the solution of (9). Since C is independent of $\boldsymbol{x}$, the original optimization problem in (9) may be approximated with

$$\underset{\boldsymbol{x}\in\mathcal{F}_2}{\text{minimize}}\quad\frac{f_1(\boldsymbol{x})}{f_2(\boldsymbol{x})}. \tag{13}$$

C. Quadratically Constrained Fractional Quadratic Program Solution

The quadratically constrained fractional quadratic program was studied in [21]. Note that $\mathbf{A}_1$ ($\mathbf{A}_1'$) and $\mathbf{A}_2$ are symmetric and there are no conditions on their definiteness. In case $\mathbf{A}_n$ ($\mathbf{A}_n'$) is not symmetric, it can be replaced by $\frac{\mathbf{A}_n+\mathbf{A}_n^{\mathrm{T}}}{2}$ ($\frac{\mathbf{A}_n'+\mathbf{A}_n'^{\mathrm{T}}}{2}$) without changing the problem. In (13), $\mathbf{A}_2\succ 0$ ($\mathbf{A}_2'\succ 0$), since it is a diagonal block of a positive definite matrix. The only assumption needed to solve (13) is that $f_2(\boldsymbol{x})$ is bounded below on $\mathcal{F}_2$ by a positive number γ. It can be seen from (5) and (7) that this assumption is trivially satisfied with $f_2(\boldsymbol{x})\geq 1$. An iterative bisection algorithm for obtaining an ϵ-global optimal solution $\boldsymbol{x}^\star$ for the problem (13) was developed in [21], specifically

$$\alpha^\star\leq\frac{f_1\left(\boldsymbol{x}^\star\right)}{f_2\left(\boldsymbol{x}^\star\right)}\leq\alpha^\star+\epsilon$$

where $\boldsymbol{x}^\star\in\mathcal{F}_2$, $\alpha^\star\triangleq\min_{\boldsymbol{x}\in\mathcal{F}_2}\{\frac{f_1(\boldsymbol{x})}{f_2(\boldsymbol{x})}\}$, and ϵ is an arbitrarily small positive number. An upper and lower bound m and M, respectively, on $\min_{\boldsymbol{x}\in\mathcal{F}_2}\{\frac{f_1(\boldsymbol{x})}{f_2(\boldsymbol{x})}\}$ must first be established.

Algorithm 1: DOP Minimization.

Given: m, M (cf., (14) and (15)), and ϵ,
Initialization: $l_0=m$, $u_0=M$,
$\Delta_{ul}=1+\epsilon$,
while $\Delta_{ul}>\epsilon$, $k\geq 1$, **do**
  $\alpha_k=\frac{l_{k-1}+u_{k-1}}{2}$,
  Solve $\underset{\boldsymbol{x}\in\mathcal{F}_2}{\text{minimize}}\ \beta_k=f_1(\boldsymbol{x})-\alpha_k f_2(\boldsymbol{x})$,
  if $\beta_k^\star\leq 0$ **then**
    $l_k\leftarrow l_{k-1}$, $u_k\leftarrow\alpha_k$,
  else
    $l_k\leftarrow\alpha_k$, $u_k\leftarrow u_{k-1}$,
  $\Delta_{ul}\leftarrow u_k-l_k$,
Return $\boldsymbol{x}^\star=\underset{\boldsymbol{x}\in\mathcal{F}_2}{\operatorname{argmin}}\ \{f_1(\boldsymbol{x})-u_k f_2(\boldsymbol{x})\}$.

The following bounds may be established on f_1 and f_2:

$$f_1(\boldsymbol{x})=\begin{cases}\boldsymbol{u}^{\mathrm{T}}\mathbf{Q}\boldsymbol{u}\leq 0,\\ \boldsymbol{u}^{\mathrm{T}}\mathbf{Q}'\boldsymbol{u}\leq 0,\end{cases},\qquad f_2(\boldsymbol{x})=1+\boldsymbol{u}^{\mathrm{T}}\mathbf{M}^{-1}\boldsymbol{u}\geq 1$$

since $\mathbf{Q}\preceq 0$, $\mathbf{Q}'\preceq 0$, and $\mathbf{M}^{-1}\succ 0$. Subsequently, m and M may be chosen to be

$$M=0,\qquad m\leq-\max_{\boldsymbol{x}\in\mathcal{F}_2}\ -f_1(\boldsymbol{x})=\begin{cases}-\max\limits_{\boldsymbol{x}\in\mathcal{F}_2} & -g_1(\boldsymbol{x})\\ -\max\limits_{\boldsymbol{x}\in\mathcal{F}_2} & -g_1'(\boldsymbol{x})\end{cases}. \tag{14}$$

Noting that $\|\boldsymbol{h}_N\|_2^2\leq h+\delta$, where $h=2$ for pseudorange measurements and $h=1$ for range measurements, the following inequality holds:

$$0\leq\|\boldsymbol{u}\|_2\leq\mu_N\sqrt{h+\delta}+\frac{1}{\mu_N}\left\|\mathbf{H}_{N-1}^{\mathrm{T}}\boldsymbol{y}_N\right\|_2.$$

Therefore, m may be chosen to be

$$m=-\begin{cases}\left[\mu_N\sqrt{h+\delta}+\frac{1}{\mu_N}\left\|\mathbf{H}_{N-1}^{\mathrm{T}}\boldsymbol{y}_N\right\|_2\right]^2\lambda_{\max}(-\mathbf{Q})\\ \left[\mu_N\sqrt{h+\delta}+\frac{1}{\mu_N}\left\|\mathbf{H}_{N-1}^{\mathrm{T}}\boldsymbol{y}_N\right\|_2\right]^2\lambda_{\max}\left(-\mathbf{Q}'\right).\end{cases} \tag{15}$$

where $\lambda_{\max}(\cdot)$ denotes the largest eigenvalue.

The following equivalency was shown in [25]

$$\min_{\boldsymbol{x}\in\mathcal{F}_2}\ \left\{\frac{f_1(\boldsymbol{x})}{f_2(\boldsymbol{x})}\right\}\leq\alpha\quad\Leftrightarrow\quad\min_{\boldsymbol{x}\in\mathcal{F}_2}\ \{f_1(\boldsymbol{x})-\alpha f_2(\boldsymbol{x})\}\leq 0.$$

This equivalency enables (13) to be solved using a bisection algorithm, which is summarized in Algorithm 1.

Next, the algorithm for minimizing $f_1(\boldsymbol{x})-\alpha f_2(\boldsymbol{x})$ is described. It can be seen that minimizing $f_1(\boldsymbol{x})-\alpha f_2(\boldsymbol{x})$ is equivalent to minimizing $\boldsymbol{x}^{\mathrm{T}}\tilde{\mathbf{A}}\boldsymbol{x}-2\tilde{\boldsymbol{b}}^{\mathrm{T}}\boldsymbol{x}+\tilde{c}$, where

$$\tilde{\mathbf{A}}\triangleq\mathbf{A}_1-\alpha\mathbf{A}_2,\qquad\tilde{\boldsymbol{b}}\triangleq\boldsymbol{b}_1-\alpha\boldsymbol{b}_2,\qquad\tilde{c}\triangleq c_1-\alpha c_2.$$

In the case of minimizing $g'(\mathbf{P}_N)$, $\mathbf{A}_n$, $\boldsymbol{b}_n$, and c_n are replaced by $\mathbf{A}_n'$, $\boldsymbol{b}_n'$, and c_n', respectively. Note that $\tilde{\mathbf{A}}$ is symmetric; therefore, it is diagonalizable with the following eigenvalue decomposition

$$\tilde{\mathbf{A}}=\mathbf{U}\Lambda\mathbf{U}^{\mathrm{T}}$$

where $\mathbf{U}$ is orthonormal and Λ is a diagonal matrix whose diagonal elements are the eigenvalues of $\tilde{\mathbf{A}}$, denoted λ_i. The eigenvalues and eigenvectors of $\tilde{\mathbf{A}}$ are reordered such that $\lambda_1 \geq \lambda_2 \geq \lambda_3$. With the change of variable $\boldsymbol{x} \triangleq \mathbf{U}\boldsymbol{s}$ and defining $\boldsymbol{w} \triangleq \mathbf{U}^{\mathsf{T}}\boldsymbol{b} = [w_1, w_2, w_3]^{\mathsf{T}}$, the following optimization problems are equivalent:

$$\begin{aligned} &\underset{\boldsymbol{x}\in\mathcal{F}_2}{\text{minimize}} \quad f_1(\boldsymbol{x}) - \alpha f_2(\boldsymbol{x}) \\ \Leftrightarrow \quad &\underset{\boldsymbol{s}\in\mathcal{F}_2}{\text{minimize}} \quad \boldsymbol{s}^{\mathsf{T}}\Lambda\boldsymbol{s} - 2\,\boldsymbol{w}^{\mathsf{T}}\boldsymbol{s} + \tilde{c}. \end{aligned} \tag{16}$$

The solution of (16) is given by $\boldsymbol{s}^\star = [s_1^\star, s_2^\star, s_3^\star]^{\mathsf{T}}$ [21], with

$$s_i^\star = \frac{w_i}{\lambda_i - \eta^\star - \xi^\star}$$

$$\left(\eta^\star, \xi^\star\right) = \begin{cases} (\bar{\eta}, 0), & \text{if } \lambda_3 \leq 0 \\ (\bar{\eta}, 0), & \text{if } \lambda_3 > 0 \text{ and } h(\bar{\eta}, 0) > h(0, \bar{\xi}) \\ \left(0, \bar{\xi}\right), & \text{otherwise,} \end{cases}$$

and $\bar{\eta}$ and $\bar{\xi}$ are the solutions to the optimization problems

$$\underset{\eta\leq\min\{\lambda_3^-, 0\}}{\text{maximize}} \quad h(\eta, 0) \tag{17}$$

$$\underset{0\leq\xi<\lambda_3}{\text{maximize}} \quad h(0, \xi) \tag{18}$$

respectively, where λ_3^- is the left-hand limit of λ_3 and

$$h(\eta, \xi) \triangleq -\sum_{i=1}^{3} \frac{w_i^2}{\lambda_i - \eta - \xi} + (1+\delta)\eta + \xi + \tilde{c}.$$

The functions $h_1(\eta) \triangleq h(\eta, 0)$ and $h_2(\xi) \triangleq h(0, \xi)$ are called secular functions [25]. These functions are strictly concave for $\eta, \xi < \lambda_3$, making (17) and (18) convex optimization problems. Therefore, one may solve for $h_1'(\eta) \equiv 0$ ($h_2'(\xi) \equiv 0$) using iterative methods (e.g., Newton's method) and if $\bar{\eta} \geq 0$ ($\bar{\xi} \leq 0$), set $\bar{\eta} \equiv 0$ ($\bar{\xi} \equiv 0$). Finally, $\boldsymbol{x}_\delta^\star$ is obtained from $\boldsymbol{x}_\delta^\star = \mathbf{U}\boldsymbol{s}^\star$ and $\boldsymbol{x}^\star$ is obtained from (12).

V. SIMULATION RESULTS

In this section, three sets of MC simulations are performed to validate the proposed approach. In the first set, described in Section V-A, the solution obtained with the proposed algorithm is plotted against the global optimal solution obtained by exhaustively sweeping the entire feasible space, showing that the solution obtained with the proposed algorithm always converges to the global optimal solution. In the second set, described in Section V-B, the solution obtained with the proposed algorithm is plotted against the solution obtained with a general-purpose solver, showing that the proposed algorithm outperforms the general-purpose solver. In the third set, described in Section V-C, the solution obtained with the proposed algorithm is plotted against the solution of an existing method that aims at maximizing the area of the polygon formed by the endpoints of the unit LOS vectors pointing from the source to the sensor [19], showing the superiority of the proposed algorithm over the method in [19]. Moreover, the proposed algorithm is evaluated in the case of source localization and simulation results, provided in Section V-E, show that the proposed algorithm always yields a lower WGDOP compared to the one obtained with a general-purpose solver.

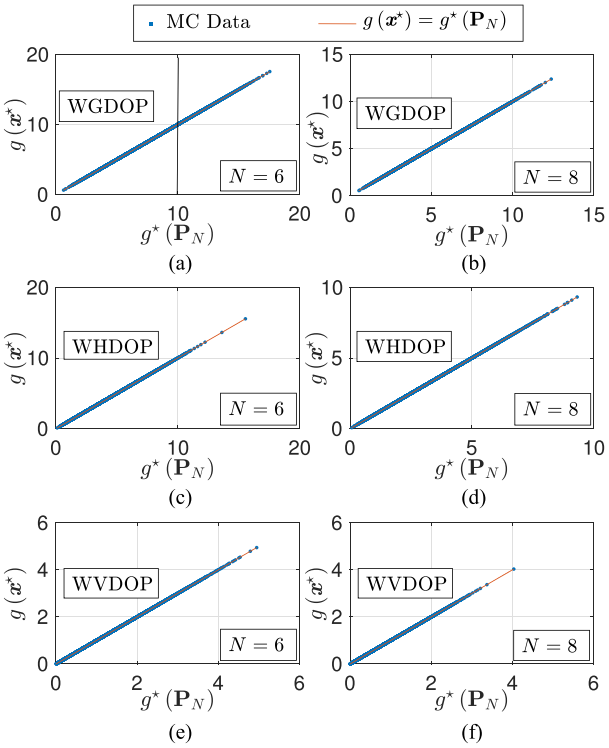

Fig. 6. MC simulation results comparing the global optimal solution $g^\star(\mathbf{P}_N)$ obtained by exhaustively sweeping the feasible set versus the optimal solution $g(\boldsymbol{x}^\star)$ obtained with the proposed approach. Results corresponding to the WGDOP, WHDOP, and WVDOP problems are given for $N = 6$ and 8 sensors. MC points are overlaid over a line defined by $g(\boldsymbol{x}^\star) = g^\star(\mathbf{P}_N)$, showing a perfect match.

A. Proposed Algorithm Versus Global Optimal Solution

In the first set of simulations, the two cost functions were evaluated for three cases: first, the WGDOP, i.e., $\mathbf{T} = \mathbf{T}' = \mathbf{I}_{4\times4}$; second, the WHDOP, i.e., $\mathbf{T} = \mathbf{T}' = [\mathbf{I}_{2\times2} \quad \mathbf{0}_{2\times2}]$; and third, the WVDOP, i.e., $\mathbf{T} = \mathbf{T}' = \boldsymbol{e}_3^{\mathsf{T}}$. For each case, 10^4 MC runs were conducted for $N = 6$ and 8. The optimal solutions computed using the proposed approach, denoted $g(\boldsymbol{x}^\star)$ and $g'(\boldsymbol{x}^\star)$, were plotted against the global optimal solutions, denoted $g^\star(\mathbf{P}_N)$ and $g'^\star(\mathbf{P}_N)$, obtained by exhaustively sweeping the entire feasible set, respectively (see Figs. 6 and 7). The positions of the $N-1$ predeployed sensors were generated randomly by drawing $N-1$ elevation angles from $\mathcal{U}(-\frac{\pi}{2}, \frac{\pi}{2})$ and $N-1$ azimuth angles from $\mathcal{U}(0, 2\pi)$, where $\mathcal{U}(a, b)$ denotes the uniform distribution with support over $[a, b]$. The measurement noise covariance $\mathbf{R}_N$ is also generated randomly at each iteration. It can be seen that the optimal solutions obtained by the proposed approach were identical to the optimal solution obtained by exhaustively sweeping the feasible set. Note that the WVDOP results for $g'(\mathbf{P}_N)$ is not plotted since in the WVDOP problem, $g(\mathbf{P}_N) = g'(\mathbf{P}_N)$.

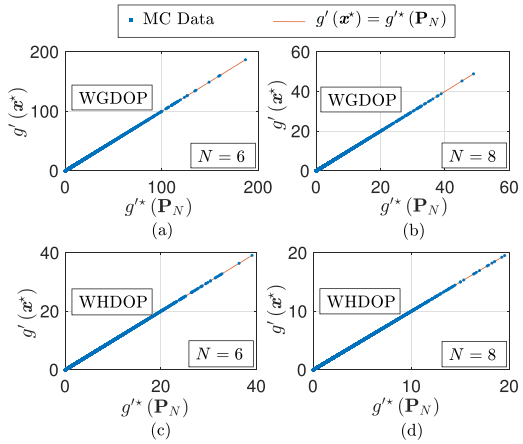

Fig. 7. MC simulation results comparing the global optimal solution $g'^\star(\mathbf{P}_N)$ obtained by exhaustively sweeping the feasible set versus the optimal solution $g'(\boldsymbol{x}^\star)$ obtained with the proposed approach. Results corresponding to the WGDOP and WHDOP problems are given for $N = 6$ and 8 sensors. MC points are overlaid over a line defined by $g'(\boldsymbol{x}^\star) = g'^\star(\mathbf{P}_N)$, showing a perfect match.

B. Proposed Algorithm Versus Nonlinear Numerical Optimization Solver Solution

In this second set of simulations, the two cost functions were evaluated for the same three cases. For each case, 10^4 MC runs were conducted for $N = 6$ and 8. The optimal solutions computed using the proposed approach was plotted against the global optimal solutions denoted $g^\star_{\texttt{fmincon}}(\mathbf{P}_N)$ and $g'^\star_{\texttt{fmincon}}(\mathbf{P}_N)$ obtained by using MATLAB's nonlinear numerical optimization solver `fmincon` (see Figs. 8 and 9). The MATLAB solver was initialized randomly. The position of the $N-1$ predeployed sensors and the measurement noise covariance $\mathbf{R}_N$ were generated the same way as in the first set of simulations. It can be seen that all MC simulation points lie either on or below the $g(\boldsymbol{x}^\star) = g^\star_{\texttt{fmincon}}(\mathbf{P}_N)$ and $g'(\boldsymbol{x}^\star) = g'^\star_{\texttt{fmincon}}(\mathbf{P}_N)$ lines, indicating that $g(\boldsymbol{x}^\star) \leq g^\star_{\texttt{fmincon}}(\mathbf{P}_N)$ and $g'(\boldsymbol{x}^\star) \leq g'^\star_{\texttt{fmincon}}(\mathbf{P}_N)$ for all MC runs. The proposed method outperforms MATLAB's `fmincon`, since `fmincon` may converge to a local minimum instead of the global minimum. Note that `fmincon` could be configured to employ one of four numerical algorithms (for the given constraints): `interior-point` (default), `sqp` (sequential quadratic program), `sqp-legacy`, and `active-set`. It was found that all four algorithms yielded $g(\boldsymbol{x}^\star) \leq g^\star_{\texttt{fmincon}}(\mathbf{P}_N)$ and $g'(\boldsymbol{x}^\star) \leq g'^\star_{\texttt{fmincon}}(\mathbf{P}_N)$ for all MC runs.

C. Proposed Algorithm Versus Area Maximization Solution

In this third set of simulations, the proposed method is compared with the method described in [19]. In [19], the authors propose to maximize the area of the polygon whose vertices are the endpoints of the unit LOS vectors pointing from the source to the sensors in a 2-D environment. Area maximization is intimately related to DOP minimization, yielding a solution that is close to the one obtained by DOP minimization. The area maximization's elegant solution is shown to be the bisector of the largest angle between consecutive sensors on the unit circle [19]. To compare against the area maximization criterion, the proposed algorithm is adapted to a 2-D envi-

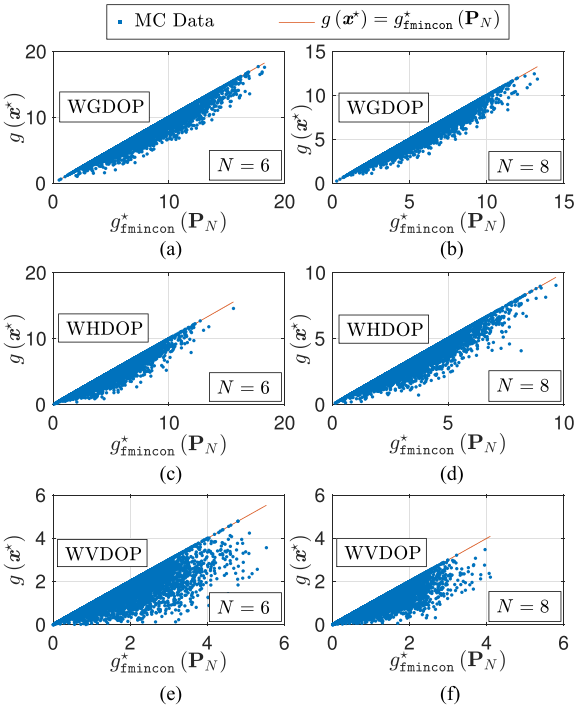

Fig. 8. MC simulation results comparing the optimal solution $g^\star_{\texttt{fmincon}}(\mathbf{P}_N)$ obtained using MATLAB's `fmincon` versus the optimal solution $g(\boldsymbol{x}^\star)$ obtained with the proposed approach. Results corresponding to the WGDOP, WHDOP, and WVDOP problems are given for $N = 6$ and 8 sensors. MC points are overlaid over or lie beneath a line defined by $g(\boldsymbol{x}^\star) = g^\star_{\texttt{fmincon}}(\mathbf{P}_N)$, showing that $g(\boldsymbol{x}^\star) \leq g^\star_{\texttt{fmincon}}(\mathbf{P}_N)$.

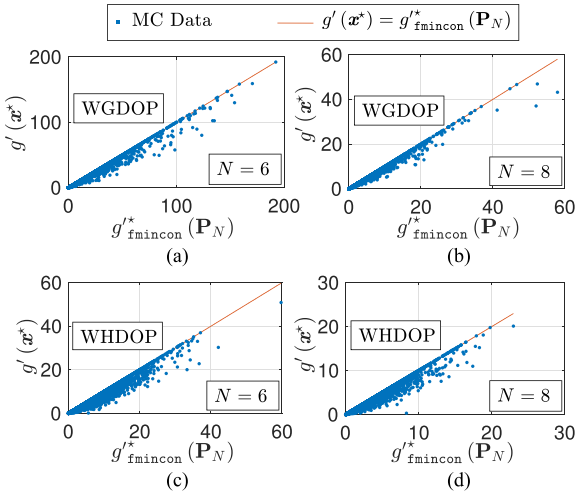

Fig. 9. MC simulation results comparing the optimal solution $g'^\star_{\texttt{fmincon}}(\mathbf{P}_N)$ obtained using MATLAB's `fmincon` versus the optimal solution $g'(\boldsymbol{x}^\star)$ obtained with the proposed approach. Results corresponding to the WGDOP and WHDOP problems are given for $N = 6$ and 8 sensors. MC points are overlaid over or lie beneath a line defined by $g'(\boldsymbol{x}^\star) = g'^\star_{\texttt{fmincon}}(\mathbf{P}_N)$, showing that $g'(\boldsymbol{x}^\star) \leq g'^\star_{\texttt{fmincon}}(\mathbf{P}_N)$.

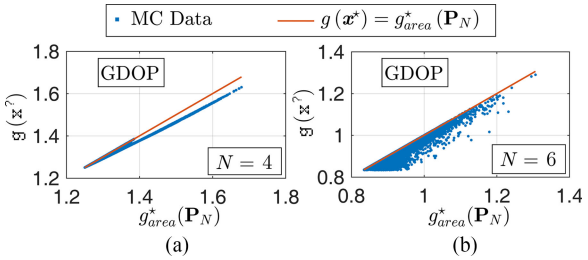

Fig. 10. MC simulation results comparing the optimal solution $g^\star_{\text{area}}(\mathbf{P}_N)$ obtained using the method proposed in [19] versus the optimal solution $g(\boldsymbol{x}^\star)$ obtained with the proposed approach. Results corresponding to the GDOP problems are given for (a) $N = 4$ and (b) $N = 6$ sensors. MC points are overlaid over or lie beneath a line defined by $g(\boldsymbol{x}^\star) = g^\star_{\text{area}}(\mathbf{P}_N)$, showing that $g(\boldsymbol{x}^\star) \leq g^\star_{\text{area}}(\mathbf{P}_N)$.

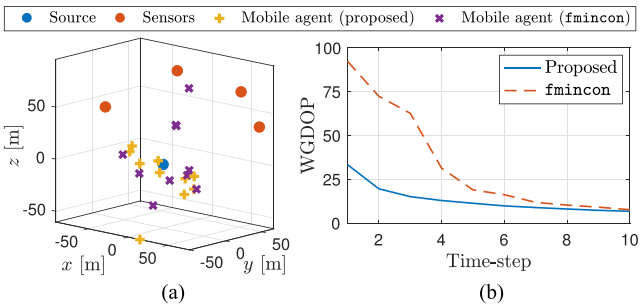

Fig. 11. Simulation results demonstrating the application of the proposed algorithm to source localization. (a) Four sensors are predeployed around a source and are making pseudorange measurements to localize it. A mobile agent is then deployed to minimize the WGDOP for 10 consecutive time-steps. (b) WGDOP results for the proposed algorithm and MATLAB's `fmincon`.

ronment, i.e., $\boldsymbol{r}_{r_j} = [x_{r_j}, y_{r_j}]^{\mathrm{T}}$ and $\boldsymbol{r}_s = [x_s, y_s]^{\mathrm{T}}$, and thus $\boldsymbol{x} = [\cos(\phi) \quad \sin(\phi)]^{\mathrm{T}}$. The cost function considered was $g(\boldsymbol{x})$ with $\mathbf{T} = \mathbf{I}_{3\times 3}$ and $\mathbf{R}_N = \mathbf{I}_{N\times N}$. A total of 10^4 MC runs were conducted for $N = 4$ and 6. The optimal solutions computed using the proposed approach were plotted against the global optimal solutions obtained using the method in [19] denoted $g^\star_{\text{area}}(\mathbf{P}_N)$ in Fig. 10. The position of the $N-1$ predeployed sensors were generated the same way as in the first two sets of simulations. It can be seen that all MC simulation points lie either on or below the $g(\boldsymbol{x}^\star) = g^\star_{\text{area}}(\mathbf{P}_N)$ lines, indicating that $g(\boldsymbol{x}^\star) \leq g^\star_{\text{area}}(\mathbf{P}_N)$ for all MC runs. It can also be seen that the proposed method outperforms the one proposed in [19].

D. Discussion

The simulation results presented in Sections V-A and V-B reveal that while general-purpose nonlinear optimal solvers could converge to a local minimum, the proposed algorithm always converges to the global minimum, regardless of the configuration of the predeployed sensors (navigation sources) or the measurement noise covariance matrix. It is important to note that initialization affects the final solution in the general-purpose nonlinear numerical optimization solver. However, there is no way of knowing where the solver must be initialized to guarantee its convergence to the global optimal solution. This justifies why `fmincon` was initialized randomly on the unit sphere. In contrast, the proposed method does not need any initialization and always converges to the global optimum. The simulation results presented in Section V-C reveal that although the area maximization problem is a good approximation of the DOP minimization problem, it does not yield a lower GDOP than the one obtained using the proposed method.

Next, the complexity of the proposed algorithm is analyzed. First, the complexity of obtaining the global minimum by exhaustively sweeping the feasible space is discussed. Consider a uniform gridding of the elevation and azimuth angles. Denote S to be the resulting number of discrete intervals in the elevation angle range. Since the azimuth angle range is twice as large as the elevation angle range, the resulting number of discrete intervals in the azimuth angle range will be $2S$. Therefore, there will be $2S^2$ feasible points to evaluate. However, the complexity of the proposed algorithm is independent of the gridding resolution. In [21], it is noted that the computationally expensive part of the proposed algorithm is computing the eigenvalues of $\tilde{\mathbf{A}}$, which has a complexity of $\mathcal{O}(n^3)$, where n is the size of the matrix. However, in the optimization problems addressed in this paper, the size of $\tilde{\mathbf{A}}$ is always 3, which means that the cost of the proposed algorithm is constant; namely $\mathcal{O}(1)$ per iteration. Therefore, as S increases, the number of feasible solutions increases quadratically, whereas the complexity of the proposed algorithm remains constant. In the previous simulation results, ϵ was chosen to be $\epsilon \equiv 10^{-7}$. In order to obtain this resolution in the exhaustive sweeping approach, S must be greater than 6.28×10^7, which is impractically large. Note that both algorithms are comparable in memory allocation and do not require a lot of memory. The simulations were conducted on a desktop computer with an Intel i7 processor clocked at 3.6 GHz with 16 GB of RAM. For $S = 128$, the sweeping algorithm iteration took on average 0.185 s, while the proposed algorithm took 0.00183 s per iteration, which is approximately 200 times faster than the sweeping algorithm.

E. Application to Source Localization

In this section, the proposed algorithm is applied to source localization with a mobile agent. To this end, four sensors were predeployed randomly around an unknown source. The sensors are making pseudorange measurements to localize the unknown source. It is desired to deploy a mobile agent that chooses its next position so to minimize the WGDOP associated with localizing the source. The diagonal elements of the measurement noise covariance were set to $\{10, 11, 9, 8, 12\}$ and all the off-diagonal elements were set to 2. The measurements taken by the sensors and the moving agent are processed in a centralized, sequential manner. After each measurement taken by the sensors and the mobile agent, the prior $\mathbf{P}_0(k)$ is updated according to

$$\mathbf{P}_0^{-1}(k+1) = \mathbf{P}_0^{-1}(k) + \mathbf{H}_N^{\mathrm{T}}(k)\mathbf{R}_N^{-1}\mathbf{H}_N(k),$$

where k is the time-step index and $\mathbf{H}_N(k)$ is the measurement Jacobian evaluated at the sensors' fixed positions and the mobile agent's current position. The mobile agent's optimal position was determined for 10 successive time-steps using the proposed algorithm as well as MATLAB's `fmincon` for comparison purposes. The simulation results are shown in Fig. 11, from which it can be seen that the proposed method outperforms `fmincon`. It is important to note that this method can also be applied to the case of a mobile source or to the case where the sensors are making range measurements to a mobile target.

VI. CONCLUSION

This paper proposed a method for obtaining a global minimum for the DOP minimization problem. Two equivalent problems were formulated, where it was assumed that an Nth sensor (navigation source) was to be added to a set of $N-1$ predeployed sensors (navigation sources) estimating the 3-D position and clock bias of a source (UAV). The additional sensor was to be placed so to minimize variations of the DOP problem (WGDOP, WHDOP, WVDOP, etc.). It was shown that the proposed cost functions are nonconvex. Subsequently, a method for obtaining the global minimum of the proposed cost functions was presented by formulating the DOP minimization problem as a quadratically constrained fractional quadratic problem. Simulation results were provided validating the global optimality of the solution obtained from the proposed algorithm. It was shown that the proposed method is superior to nonlinear numerical optimization solvers, that often converge to local optima. Moreover, it was shown that the proposed method outperforms the area maximization criterion.

JOE J. KHALIFE, *Student Member, IEEE*
University of California, Riverside, USA

ZAHER (ZAK) M. KASSAS, *Senior Member, IEEE*
University of California, Riverside, USA

REFERENCES

[1] J. Kim and S. Sukkarieh
Autonomous airborne navigation in unknown terrain environments
IEEE Trans. Aerosp. Electron. Syst., vol. 40, no. 3, pp. 1031–1045, Jul. 2004.

[2] K. Dogancay
UAV path planning for passive emitter localization
IEEE Trans. Aerosp. Electron. Syst., vol. 48, no. 2, pp. 1150–1166, Apr. 2012.

[3] S. Monica and G. Ferrari
UWB-based localization in large indoor scenarios: optimized placement of anchor nodes
IEEE Trans. Aerosp. Electron. Syst., vol. 51, no. 2, pp. 987–999, Apr. 2015.

[4] S. Martinez and F. Bullo
Optimal sensor placement and motion coordination for target tracking
Automatica, vol. 42, no. 4, pp. 661–668, Apr. 2006.

[5] K. Punithakumar, T. Kirubarajan, and M. Hernandez
Multisensor deployment using PCRLBS, incorporating sensor deployment and motion uncertainties
IEEE Trans. Aerosp. Electron. Syst., vol. 42, no. 4, pp. 1474–1485, Oct. 2006.

[6] C. Yang, L. Kaplan, E. Blasch, and M. Bakich
Optimal placement of heterogeneous sensors for targets with Gaussian priors
IEEE Trans. Aerosp. Electron. Syst., vol. 49, no. 3, pp. 1637–1653, Jul. 2013.

[7] F. Penna, M. Caceres, and H. Wymeersch
Cramér-Rao bound for hybrid GNSS-terrestrial cooperative positioning
IEEE Commun. Lett., vol. 14, no. 11, pp. 1005–1007, Nov. 2010.

[8] Z. Kassas, A. Arapostathis, and T. Humphreys
Greedy motion planning for simultaneous signal landscape mapping and receiver localization
IEEE J. Sel. Topics Signal Process., vol. 9, no. 2, pp. 247–258, Mar. 2015.

[9] Z. Kassas and T. Humphreys
Receding horizon trajectory optimization in opportunistic navigation environments
IEEE Trans. Aerosp. Electron. Syst., vol. 51, no. 2, pp. 866–877, Apr. 2015.

[10] J. Spilker, Jr.
"Satellite Constellation and Geometric Dilution of Precision," in *Global Positioning System: Theory and Applications*, Washington, DC, USA: Amer. Inst. Aeronaut. Astronaut., 1996, ch. 5, pp. 177–208.

[11] N. Levanon
Lowest GDOP in 2-D scenarios
IEE Proc. Radar, Sonar Navigat., vol. 147, no. 3, pp. 149–155, Jun. 2000.

[12] I. Sharp, K. Yu, and Y. Guo
GDOP analysis for positioning system design
IEEE Trans. Veh. Technol., vol. 58, no. 7, pp. 3371–3382, Sep. 2009.

[13] N. Blanco-Delgado and F. Nunes
Satellite selection method for multi-constellation GNSS using convex geometry
IEEE Trans. Veh. Technol., vol. 59, no. 9, pp. 4289–4297, Nov. 2010.

[14] R. Santerre, A. Geiger, and S. Banville
Geometry of GPS dilution of precision: revisited
Proc. IEEE, vol. 21, no. 4, pp. 1747–1763, Oct. 2017.

[15] S. Xu and K. Dogancay
Optimal sensor placement for 3-D angle-of-arrival target localization
IEEE Trans. Aerosp. Electron. Syst., vol. 53, no. 3, pp. 1196–1211, Jun. 2017.

[16] P. Massat and K. Rudnick
Geometric formulas for dilution of precision calculations
J. Inst. Navigat., vol. 37, no. 4, pp. 379–391, 1990.

[17] N. Blanco-Delgado, F. Nunes, and G. Seco-Granados
Relation between GDOP and the geometry of the satellite constellation
In *Proc. Int. Conf. Localization GNSS*, Jun. 2011, pp. 175–180.

[18] J. Morales and Z. Kassas
Optimal receiver placement for collaborative mapping of signals of opportunity
In *Proc. ION GNSS Conf.*, Sep. 2015, pp. 2362–2368.

[19] J. Morales and Z. Kassas
Optimal collaborative mapping of terrestrial transmitters: Receiver placement and performance characterization
IEEE Trans. Aerosp. Electron. Syst., vol. 54, no. 2, pp. 992–1007, Apr. 2018.

[20] J. Morales, J. Khalife, and Z. Kassas
GNSS vertical dilution of precision reduction using terrestrial signals of opportunity
In *Proc. ION Int. Tech. Meeting Conf.*, Jan. 2016, pp. 664–669.

[21] A. Beck, A. Ben-Tal, and M. Teboulle
Finding a global optimal solution for a quadratically constrained fractional quadratic problem with applications to the regularized total least squares
SIAM J. Matrix Anal. Appl., vol. 28, no. 2, pp. 425–445, May 2006.

[22] J. Morales, J. Khalife, and Z. Kassas
Opportunity for accuracy
GPS World Mag., vol. 27, no. 3, pp. 22–29, Mar. 2016.

[23] Z. Kassas, J. Khalife, K. Shamaei, and J. Morales
I hear, therefore I know where I am: Compensating for GNSS limitations with cellular signals
IEEE Signal Process. Mag., vol. 34, no. 5, pp. 111–124, Sep. 2017.

[24] Z. Kassas and T. Humphreys
Observability analysis of opportunistic navigation with pseudorange measurements
In *Proc. AIAA Guid., Navigat., Control Conf.*, Aug. 2012, vol. 1, pp. 1209–1220.

[25] W. Dinkelbach
On nonlinear fractional programming
Manage. Sci., vol. 13, no. 7, pp. 492–498, Mar. 1967.